Edge Hole Effect on Isolation of UWB MIMO RDRA for 5G Outdoor Applications

Tamer G. Abouelnaga and Esmat A. Abdallah

Microstrip Circuits Department, Electronics Research Institute ERI, Cairo, Egypt
Tamer@eri.sci.eg

***Abstract* –** For 5G sub-6 GHz outdoor applications, a highly isolated two-port rectangular dielectric resonator antenna (RDRA) with UWB MIMO is presented in this research. For isolation enhancement purposes at the lower frequency band (2.27 GHz-2.62 GHz), a longitudinal slot is inserted at the ground plane. For isolation enhancement at the higher frequency band (3.9 GHz-5.73 GHz), an edged hole is inserted in the RDRA. Investigations are conducted on the impacts of slotted ground as well as edged hole radius on isolation. The orthogonal feeding scheme of UWB MIMO RDRA considering both edged hole and slotted ground plane effects are investigated. For the edged hole MIMO RDRA with a slotted ground plane, isolation is better than -24.7 dB at a higher frequency band and is better than -15.5 dB at a lower frequency band. This isolation improvement is explained by the surface current density distribution. The use of an edged hole RDRA and an aperture-coupled orthogonal feeding allows UWB bandwidth and good efficiency performances on the 5G operating bands. To justify the MIMO performance, the envelope correlation coefficient (ECC) and diversity gain (DG) are applied.

***Index Terms* –** 5G, co-polarization, cross-polarization, DG, DRA, ECC, MIMO antenna, UWB.

I. INTRODUCTION

The primary requirements of wireless 5G communication networks are extremely high data rates, improved spectral efficiency, lower latency, and high quality of service (QoS) [1–3]. The millimeter wave frequencies (more than 24 GHz) are used for interior coverage, whereas the 5G sub-6 GHz channels are used for outdoor applications [4]. According to the most recent edition of the 3GPP technical standard (TS 38.101), the sub-6 GHz bands for 5G communications are divided into new radio bands such as n46 (5.150- 5.925), n47 (5.855-5.925), n53 (2.483.5-2.495), n77 (3.3 GHz-4.2 GHz), and n79 (4.4 GHz-5 GHz) [5]. The multiple input, multiple output (MIMO) antenna system takes into account many antenna elements on a single substrate, which worsens the isolation properties. Low isolation (below 10 dB) between antenna components with constrained spacing is therefore extremely difficult [6]. There have been many different isolation techniques used, but it has been found that decoupling networks [7–9], parasitic methods [10–12], flawed ground structures [13–15], neutralization lines [16–18], metamaterials [19–20], the self-isolated antenna [21], and orthogonal polarization [22] all resulted in better isolation. Although some of the previously suggested antennas had certain shortcomings, overall, they had a positive influence on MIMO antenna isolation. For instance, a decoupling network-used antenna [7] suffered from an increase in envelope correlation coefficient (ECC) from 0.01 and 0.19 to 0.12 and 0.29, respectively, with and without the use of a dual-band decoupling network. Frequency shifting from 5.8 GHz to 5.5 GHz was a problem for parasitic approaches [11] when electromagnetic band gap (EBG) structures were present. Due to H-shaped defected ground structures (DGS), DGS [14] only experienced little radiation profile distortion. Wider lower-frequency bandwidth as opposed to upper-frequency bandwidth was a problem for neutralization lines [18]. The susceptibility of resonators to the horizontal movement was a problem for metamaterials [19]. Hence, a mutual coupling decrease was not seen. Narrow bandwidth was a problem for orthogonal polarization and self-isolated antenna techniques [21, 22].

With isolation greater than -24.7 dB at higher frequency bandwidth (3.9 GHz to 5.73 GHz) and isolation better than -15.5 dB at lower frequency bandwidth (2.27 GHz to 2.62 GHz), a high isolated dual-port ultra-wideband (UWB) MIMO rectangular dielectric resonator antenna (RDRA) is suggested in this research. This is accomplished by using an orthogonal feeding system, an edged hole at the RDRA, and a longitudinal slot at the ground. An investigation is done into how orthogonal feeding and the effects of edged hole radius and slotted ground affect isolation. A microstrip-matched stub feed is utilized for impedance matching. An etched Z-shape aperture at the ground plane connects a dielectric resonator to a feed stub. Calculated ECC and DG both fall within the permitted range. The suggested

Submitted On: October 22, 2022
Accepted On: June 16, 2023

https://doi.org/10.13052/2023.ACES.J.380706

MIMO antenna is a candidate for sub-6 GHz outdoor 5G applications since the measured -6 dB operating frequency bandwidth is adequate for the n46, n47, n53, n77, n78, and n79 5G frequency bands.

The proposed edged hole MIMO RDRA with a slotted ground plane achieves -15.53 dB and -24.7 dB at lower and higher frequency bands, respectively. That is achieved without using DGS or EBG structures, or parasitic methods that may cause radiation distortion or frequency shift. Also, ECC is kept lower than 0.01 all over the operating lower and higher bandwidths. The proposed edged hole MIMO RDRA with a slotted ground plane has wider upper-frequency bandwidth as compared to lower-frequency bandwidth.

II. RDRA's ORTHOGONAL FEEDING METHOD

This section introduces the RDRA both without and with the slotted ground plane. The perspective view, top view, and bottom view of the MIMO RDRA are displayed in Fig. 1. It uses a low-cost FR4 substrate with a 1.6 mm thickness, a dielectric constant ε_r of 4.65, and a loss tangent $tan(\delta)$ of 0.02. On the substrate's top surface, two Z-slots and two 50 Ω matching stubs are etched into the ground plane. On the top surface of the substrate, two rectangular-shaped dielectric resonators made of alumina are positioned. The RDRA's TE_{111} mode presence is based on [23–25]. The DRA with the dimension's width w, length l, and height h emits magnetic dipole radiation. The following formulas can be used to calculate the resonant frequency:

$$f_o = \frac{c}{2\pi\sqrt{\varepsilon_r}}\sqrt{k_x^2+k_y^2+k_z^2} \quad (1)$$

$$k_x = \pi/l, k_z = \pi/2h \quad (2)$$

$$w = \frac{2}{k_y} tanh\left(\frac{k_{yo}}{k_y}\right), k_{yo} = \sqrt{k_x^2+k_z^2}, \quad (3)$$

where c represents the vacuum-bound speed of light. You may get the resonance frequency f_o by knowing the length l and height h and solving for k_y and w. The computed resonance frequency of a DRA with identical dimensions of length and breadth of 25 mm and various heights h values is shown in Table 1.

Table 1: The resonant frequency of various height levels of RDRA

h (mm)	10	15	20	25
f_o(GHz)	3.23	2.71	2.22	2.39

A dielectric cube with a 25 mm edge length is employed as a starting point. The suggested MIMO RDRA is modeled, simulated, and optimized using the CST electromagnetic solver taking into account the feeding scheme impact; the MIMO RDRA optimized dimensions are shown in Table 2. The resonance frequency for an RDRA with equal dimensions of 21.5 mm in width, length, and height is discovered to be 2.39 GHz. Without taking into account the impact of the feeding mechanism, the predicted resonant frequency is discovered to be 2.99 GHz. Figure 1 depicts the isolation between the two ports of the MIMO RDRA aerial. It is noted that at the lower operating bandwidth (2.25 GHz to 2.52 GHz), the isolation between the two ports is maintained below -9.5 dB, while at the higher operating frequency bandwidth, it is maintained below -16 dB. (3.6 GHz to 5.7 GHz).

Table 2: MIMO RDRA dimensions (mm)

L_{DRA}	S_{1H}	S_{2H}	S_{3H}	S_{1V}
21.5	18.9	17.9	7.9	9.25
S_{2V}	L_S	w_S	H_{DRA}	$L_{1\ Slot}$
11.25	80	40	15.24	11
$L_{2\ Slot}$	$L_{3\ Slot}$	$w_{1\ Slot}$	$w_{2\ Slot}$	$L_{3\ Feed}$
5	11	6	6.3	13
$L_{2\ Feed}$	$L_{1\ Feed}$	$w_{1\ Feed}$	$w_{2\ Feed}$	S_{4H}
6	7	2.7	2.7	17.3
L_{s1}	L_{s2}			
38	38			

For the lower frequency band isolation enhancement, a longitudinal slot at the ground is inserted. The obtained isolation is better than -13.2 dB, while the higher frequency band is better than -17 dB, as shown in Fig. 1 (g). The rectangular slot is etched and centered at the ground plane with dimensions of 40 mm width and

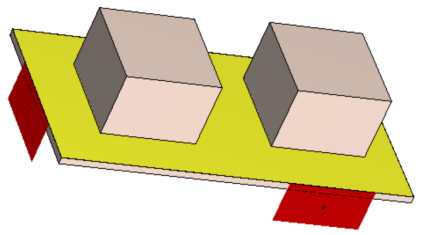

(a)

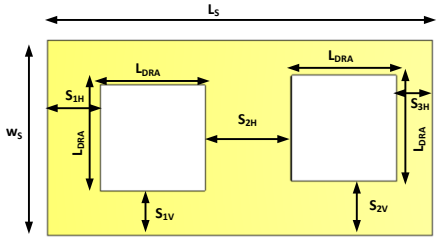

(b)

Fig. 1. *Continued*

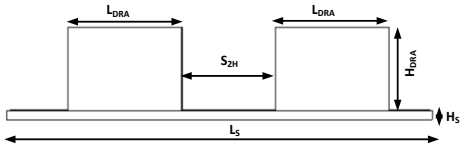

(c)

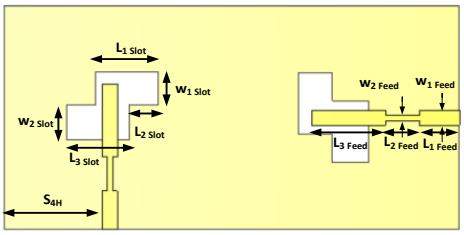

(d)

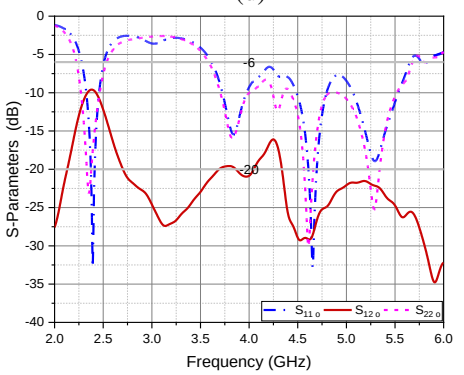

(e)

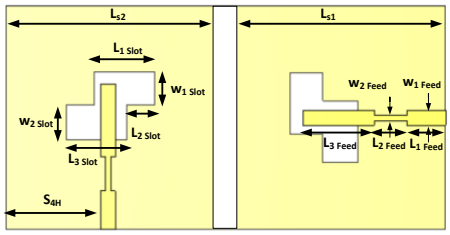

(f)

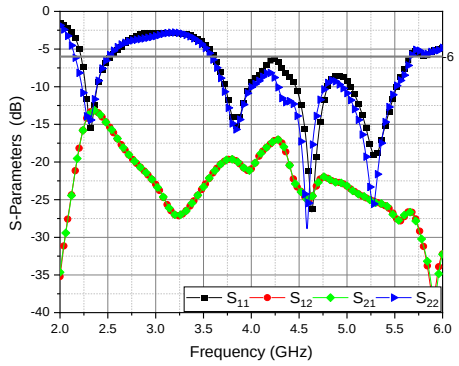

(g)

Fig. 1. The suggested MIMO RDRA: (a) perspective view, (b) top view, (c) side view, (d) bottom view, (e) S-parameters, (f) bottom view of the MIMO RDRA with the slotted ground plane, and (g) S-parameters of the MIMO RDRA with the slotted ground plane.

8.1 mm length. Its position is tuned using the CST simulator and is shown in Fig. 1 (f). Table 2 shows the dimensions of the bottom view of the slotted ground plane.

III. AN EDGED HOLE RDRA ORTHOGONAL FEEDING TECHNIQUE

This section introduces the edged hole RDRA both without and with the slotted ground plane. An edged hole of 4 mm radius is created at the RDRA edge, as illustrated in Figs. 2 (a) and (b) to improve isolation at the higher frequency band. At a higher frequency range, in Fig. 2 (c), more isolation is achieved. In comparison to -9.5 and -19.6 dB, with the same orthogonal feeding but without an edged hole and slotted ground plane, the isolation is retained below -10.5 dB and -22.3 dB at the lower and higher working bands, respectively.

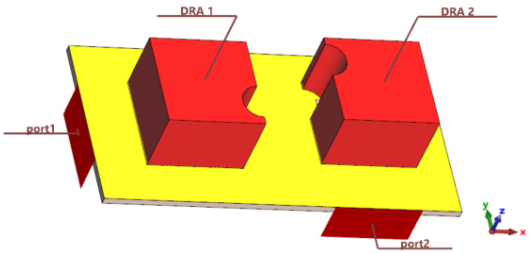

(a)

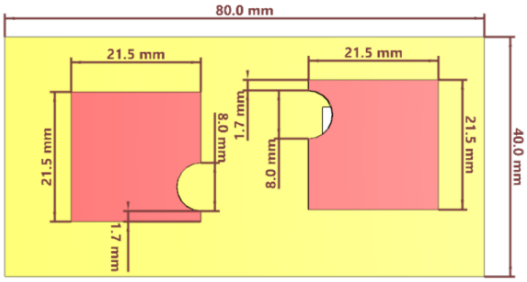

(b)

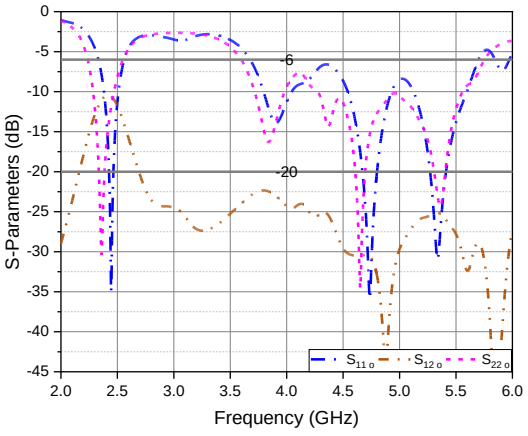

(c)

Fig. 2. The edged hole MIMO RDRA: (a) perspective view, (b) top view, and (c) S-parameters.

The impact of hole radius on isolation is seen in Fig. 3 (a). For the lower frequency range, the isolation is maintained below -9.6 dB at a hole radius of 1 mm and below -10.96 dB at a hole radius of 5 mm. Moreover, the isolation is maintained below -16.5 dB at a 1 mm hole radius and below -23.5 dB at a 5 mm hole radius at the higher frequency spectrum. At a hole radius of 1 mm, the lower bandwidth changes from 2.29 GHz-2.51 GHz to 2.36 GHz-59 GHz. According to Fig. 3 (b), the higher bandwidth changes from 3.62 GHz to 5.66 GHz at a 1 mm hole radius to 3.69 GHz to 5.74 GHz at a 5 mm hole radius.

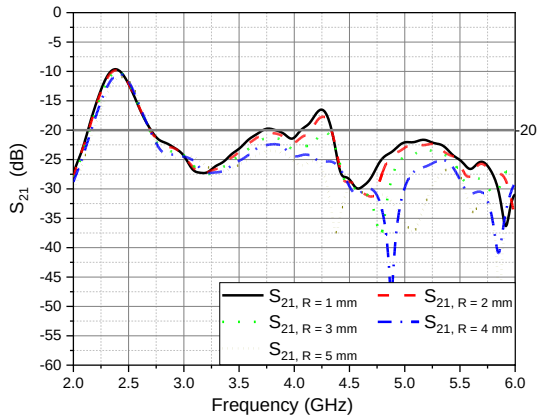

(a)

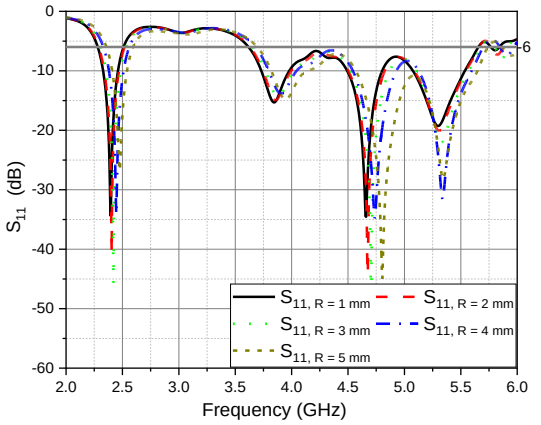

(b)

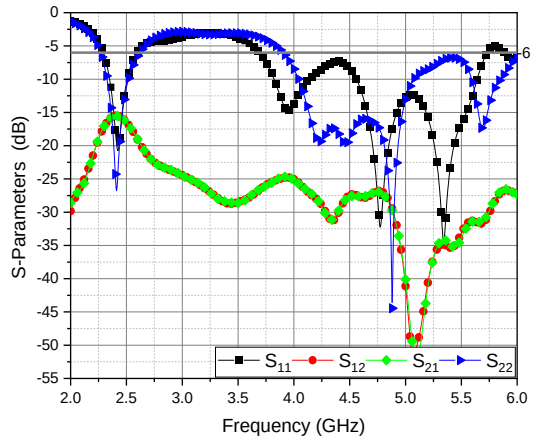

(c)

Fig. 3. MIMO edged hole RDRA: (a) S_{21}, (b) S_{11} as the hole radius varies, and (c) S-parameters with the slotted ground plane.

To achieve better isolation at the lower frequency band, the slotted ground plane is used. The same dimensions and position as Fig. 2 (f) are considered. The isolation of the higher bandwidth is kept below -24.7 dB and the lower bandwidth is kept below -15.53 dB, Fig. 3 (d). Table 3 shows the lower and the higher bandwidths along with the obtained isolation for the four previous MIMO RDRA configurations. The lower frequency band shifts from 2.25 GHz-2.52 GHz to 2.27 GHz-2.62 GHz and isolation shifts from -9.5 dB to -15.53 dB for the RDRA without the slotted ground plane and the edged hole RDRA with the slotted ground plane, respectively. Also, the higher frequency band shifts from 3.6 GHz-5.7 GHz to 3.9 GHz-5.73 GHz, and isolation shifts from -16 dB to -24.7 dB for the RDRA without the slotted ground plane and the edged hole RDRA with the slotted ground plane, respectively.

Table 3: The bandwidths and the isolations of the four MIMO RDRA configurations

Antenna	BW (GHz)	Min Isolation (dB)
RDRA without slotted ground	2.25-2.52	-9.5
	3.6-5.7	-16
RDRA with slotted ground	2.22-2.5	-13.2
	3.58-5.67	-17
Edged RDRA without slotted ground	2.33-2.56	-10.5
	3.68-5.7	-22.3
Edged RDRA with slotted ground	2.27-2.62	-15.53
	3.9-5.73	-24.7

A. Distribution of surface current

The surface current density distribution at 2.48 GHz (lower frequency band) and 4.2 GHz (higher frequency band) for both MIMO RDRA without slotted ground and MIMO edged hole RDRA with the slotted ground plane, where port 1 is excited, is shown in Fig. 4 to examine the isolation properties of the MIMO RDRA antennas. It has been noted from Fig. 4 (a) that the coupling current among MIMO components is quite weak in the case of only left MIMO RDRA excitation. The difference between the surface current density near the left RDRA and near the right RDRA, seen in Fig. 4 (a), is also higher than the difference between the surface current density near the left RDRA and near the right RDRA, shown in Fig. 4 (b). So, both surface current distribution

characteristics back up the conclusion that the suggested orthogonal MIMO RDRA's self-isolation with an edged hole structure is superior to that of the proposed orthogonal MIMO RDRA without an edged hole structure. That explains the isolation improvement that is gained when orthogonal MIMO RDRA with an edged hole structure is applied. The same outcomes have been seen when just right MIMO RDRA excitation is used, as illustrated in Fig. 4 (c) and (d).

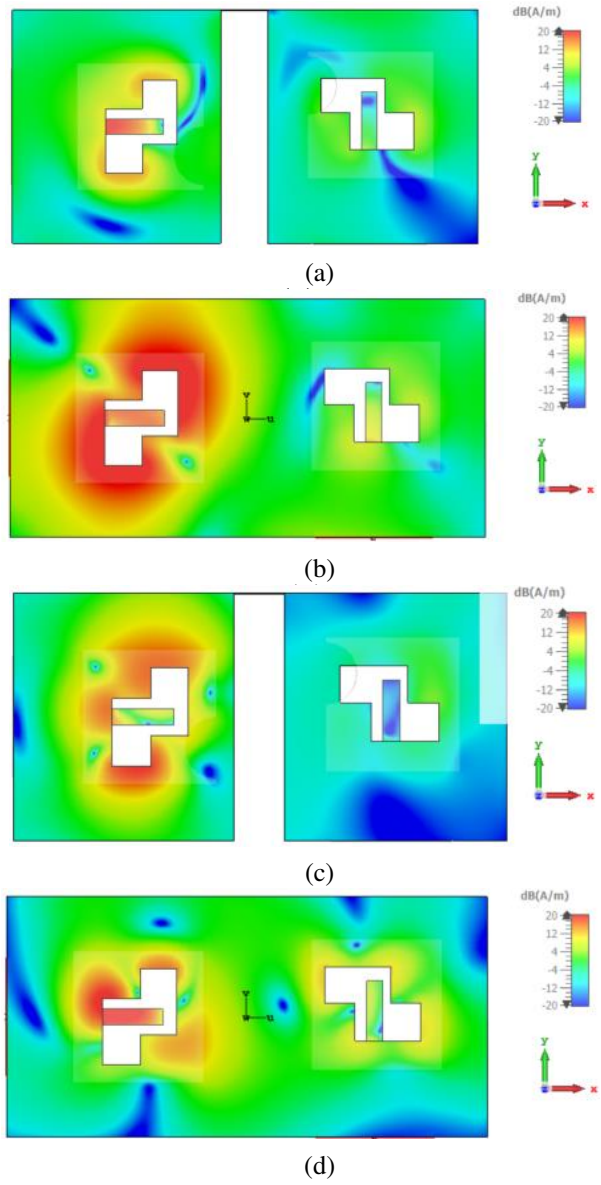

Fig. 4. Surface current distribution of MIMO RDRA: (a) with edged hole and slotted ground at 2.4 GHz, (b) without the edged hole and slotted ground at 2.4 GHz, (c) with edged hole and slotted ground at 4.2 GHz, and (d) without the edged hole and slotted ground at 4.2 GHz.

B. Co-polarized and cross-polarized radiation pattern

Resonance frequencies at 2.39 GHz, 3.84 GHz, 4.65 GHz, and 5.27 GHz are provided by the MIMO RDRA without an edged hole and slotted ground. Figure 5 shows that the proposed antenna's E-plane and H-plane radiation patterns are directional at a frequency of 2.39 GHz. (the same performance at other resonant frequencies). Moreover, Fig. 6 shows the predicted radiation pattern for the MIMO-edged hole RDRA with the slotted ground. With its slotted ground and MIMO-edged holes, the RDRA offers resonance frequencies of 2.4 GHz,

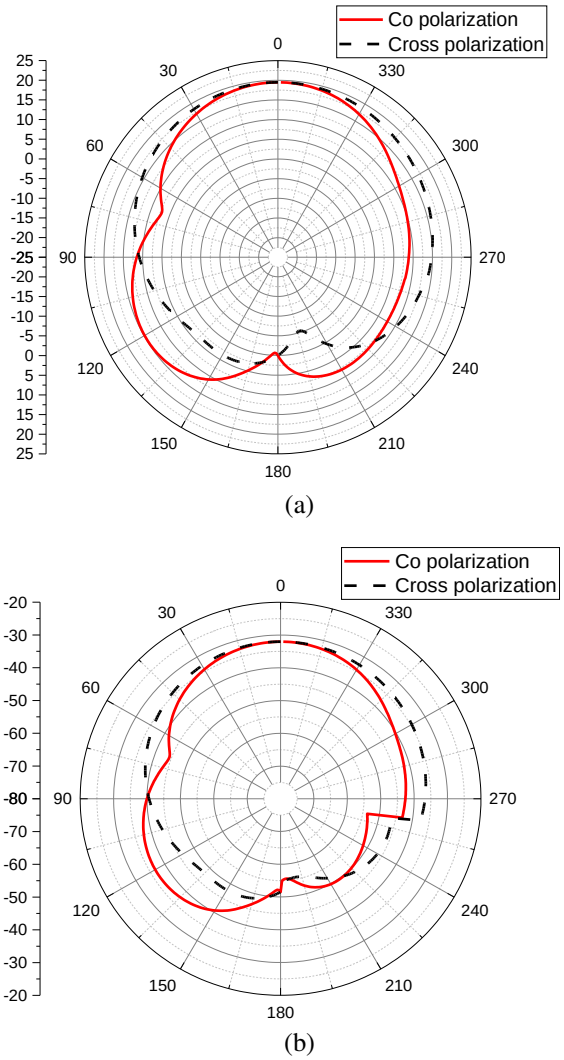

Fig. 5. MIMO RDRA antenna's simulated radiation pattern (without the edged hole and slotted ground): (a) E-plane Co and cross-polarization dB (V/m) at 2.39 GHz, and (b) H-plane Co and cross-polarization dB $(\mathrm{A/m})$ at 2.39 GHz.

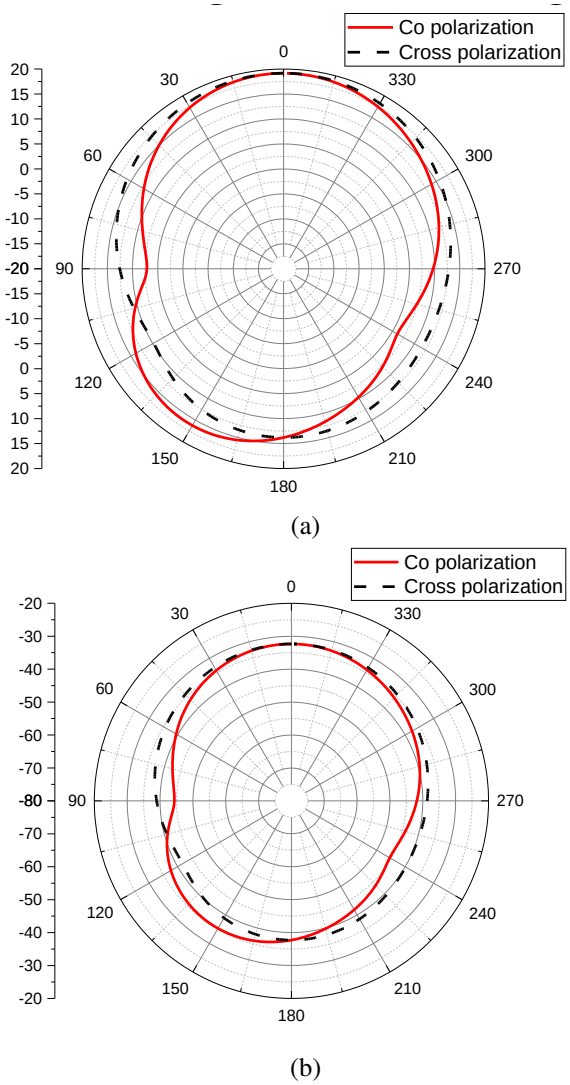

Fig. 6. MIMO RDRA antenna's simulated radiation pattern (with edged hole and with slot): (a) E-plane Co and cross-polarization dB $(\mathrm{V/m})$ at 2.4 GHz, and (b) H-plane Co and cross-polarization dB $(\mathrm{A/m})$ at 2.4 GHz.

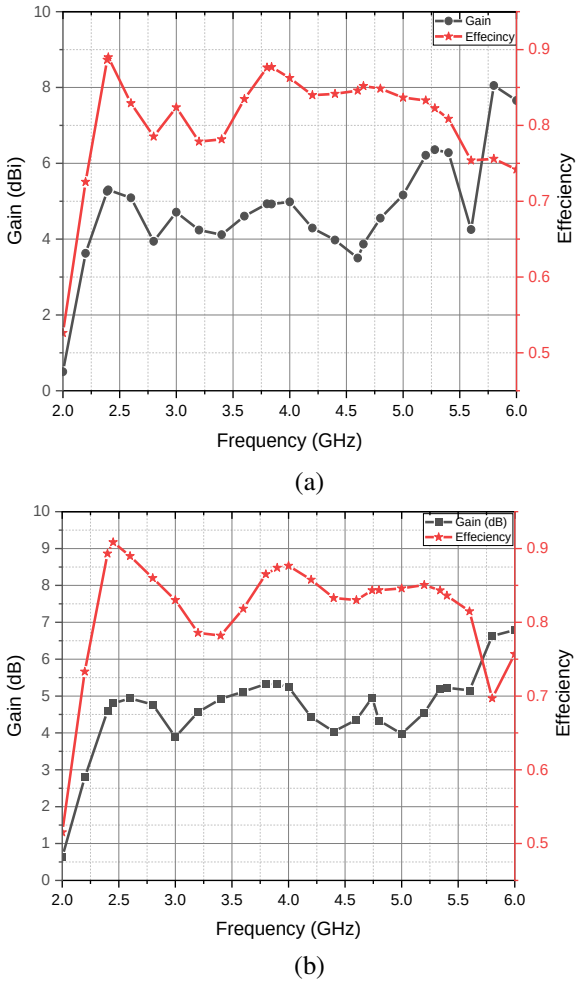

Fig. 7. Gain and radiation efficiency of MIMO RDRA: (a) without, and (b) with an edged hole and slotted ground.

3.95 GHz, 4.78 GHz, and 5.34 GHz. Co-polarization and cross-polarization are only displayed for the left MIMO-edged hole RDRA at 2.4 GHz. The radiation patterns show that the proposed antenna's E- and H-planes are directional at these resonance frequencies. Both MIMO-edged hole RDRA with and without slotted ground structures can receive signals in both directions.

In Figs. 7 (a) and (b), respectively, the simulated gain and radiation efficiency of MIMO RDRA with slotted ground and MIMO edged hole RDRA without slotted ground are shown. The radiation efficiency for MIMO RDRA without slotted ground is better than 84% for the lower operating frequency bandwidth (2.25 GHz to 2.55 GHz) and higher than 75% for the higher operating frequency bandwidth (3.6 GHz to 5.7 GHz). Radiation efficiency is better than 85% for MIMO-edged hole RDRA with the slotted ground for the lower operating frequency bandwidth (2.27 GHz to 2.62 GHz) and higher than 76% for the higher operating frequency bandwidth (3.9 GHz to 5.73 GHz). The gain for MIMO RDRA without slotted ground is higher than 4.7 dB for the lower operating frequency bandwidth (2.25 GHz to 2.55 GHz) and higher than 3.6 dB for the larger operating frequency bandwidth (3.6 GHz to 5.7 GHz). The gain is larger than 4.5 dB for MIMO-edged hole RDRA with the slotted ground for the lower operating frequency bandwidth (2.27 GHz to 2.62 GHz) and greater than 4 dB for the higher operating frequency bandwidth (3.9 GHz to 5.73 GHz).

C. Performance of diversity

By computing the diversity performance parameters (ECC, DG), the performance of the orthogonal MIMO

RDRA with and without edged holes is presented. Equation (4) is used to calculate the ECC based on the S-parameters calculation [25].

$$ECC=\frac{|S_{nn}^{*}S_{nm}+S_{mn}^{*}S_{mm}|^{2}}{\left(\left(1-(|S_{nn}|^{2}+|S_{mn}|^{2}\right)\right)\left(1-(|S_{mm}|^{2}+|S_{nm}|^{2})\right)}. \quad (4)$$

According to the International Telecommunication Union (ITU) standard, the ECC value should be smaller than 0.5 to provide optimal MIMO aerial performance. Throughout the whole operational lower and higher frequency bands, the correlation values for the MIMO RDRA without slotted ground and the edged hole RDRA with slotted ground are less than 0.04 and 0.02, respectively, making it a viable MIMO antenna for the authorized bands. Equation (5) is used to determine diversity gain [26]. Close to 10 is the acknowledged diversity gain value. Based on Fig. 8, it can be shown that

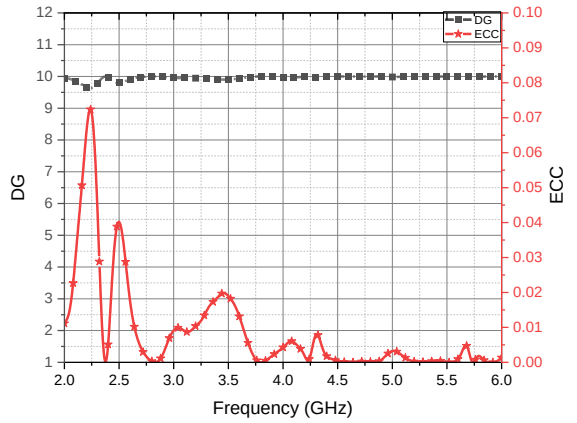

(a)

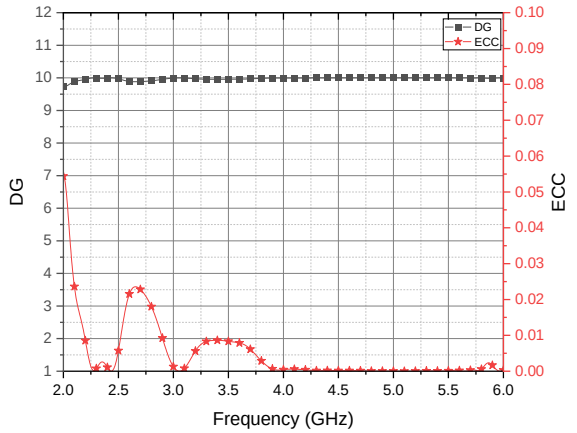

(b)

Fig. 8. ECC and DG versus frequency plot of MIMO RDRA: (a) without the slotted ground, and (b) with the edged hole and slotted ground.

for both the lower and higher operating frequency bands, MIMO RDRA without ground slot and MIMO edged hole RDRA with grounded slot both exhibit a diversity gain of almost 10.

$$DG=10\sqrt{1-|0.99ECC|^{2}}. \quad (5)$$

Table 4 shows a comparison of the proposed edged hole MIMO RDRA with a slotted ground plane considering bandwidth, isolation, ECC, and diversity gain.

Table 4: Comparison of the proposed edged hole MIMO RDRA with the previous MIMO structure

Antenna	**−6 dB** BW (**GHz**)	Min Isolation (**dB**)	Max ECC	Min DG
Edged RDRA with slotted ground	2.27–2.62	15.53	0.01	10
	3.9 – 5.73	24.7	0.002	10
[1]	3.38–3.78	26	0.04	-
	4.95–	25	0.06	-
[4]	5.58			
[8]	3.3 – 5	19	0.018	-
[15]	2.6 – 3.6	14	0.21	10

IV. PROTOTYPE OF ANTENNA

An orthogonal MIMO RDRA (without an edged hole) antenna is selected to be manufactured and tested for verification, as shown in Fig. 9. Figures 9 (a) and (b) show images of the manufactured rectangular MIMO antenna. Figure 9 (c) also displays a picture of the experimental setup. For experimental validation, a Rohde & Schwarz ZVP 20 Vector Network Analyzer is employed. Figure 10 displays the predicted and observed scattering characteristics for the suggested orthogonal MIMO-RDRA (without edged hole). The findings of the measured and simulated S-parameters coincide rather well. The relevant difference results from manufacturing flaws, soldering effects, glue effects, and an alignment issue with both the feeding system and RDRA. The RDRA block is just an alumina layer that is stacked one to another using glue. Compared to its simulated counterpart's lower frequency -6 dB bandwidth of 2.25 GHz to 2.52 GHz, the measured lower -6 dB frequency bandwidth is enlarged from 2.54 GHz to 2.79 GHz. In contrast to its simulated equivalent, which has a high-frequency -6 dB bandwidth of 3.6 GHz to 5.7 GHz, the measured -6 dB high-frequency bandwidth is expanded to 3.77 GHz to 6 GHz.

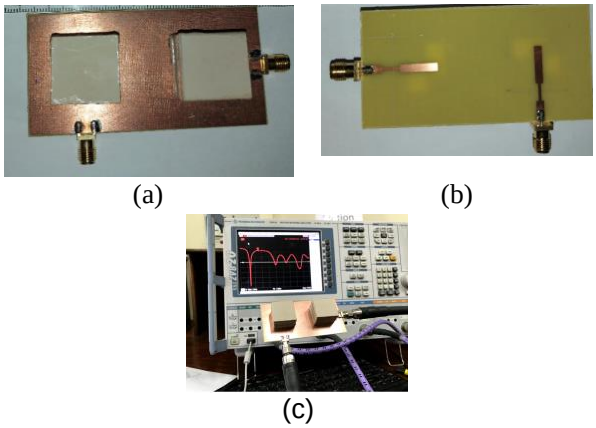

Fig. 9. Fabricated rectangular MIMO RDRA prototype (without edged hole): (a) top view, (b) bottom view, and (c) experimental setup.

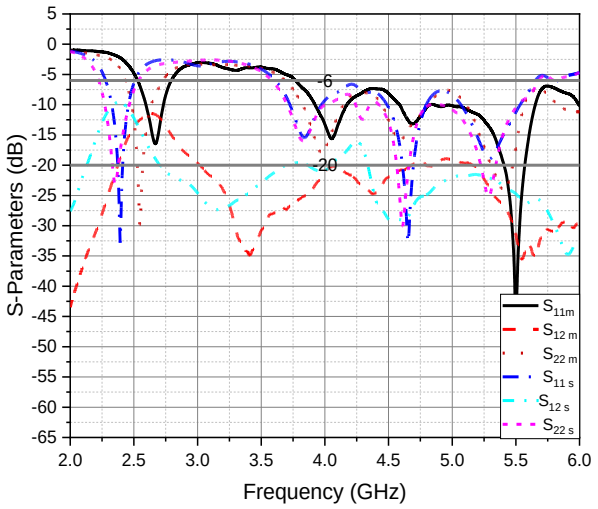

Fig. 10. Simulated and measured S-parameters of MIMO RDRA (without edged hole).

V. CONCLUSION

In this paper, MIMO RDRA with and without a slotted ground plane and MIMO edged hole RDRA with and without a slotted ground plane are investigated for an orthogonal feeding scheme. For isolation enhancement at the lower frequency band, the slotted ground plane was used, while the isolation enhancement at the higher frequency was achieved by using the edged hole RDRA.

Without a slotted ground plane, the MIMO RDRA featured two -6 dB impedance bandwidths, a lower operating frequency band (between 2.25 and 2.52 GHz), and a higher operating frequency band (3.6 GHz to 5.7 GHz). A lower operating frequency bandwidth (2.27 GHz to 2.62 GHz) and a larger operating frequency bandwidth were available for the MIMO edged hole RDRA with the slotted ground plane (3.9 GHz to 5.73 GHz). It was looked into how hole radius affected everything. Structures using MIMO RDRA have a minimum efficiency of 75%. The suggested MIMO RDRA antennas were excellent candidates for outdoor 5G applications due to the diversity of 10 throughout the working frequency bands.

REFERENCES

[1] T. G. Abouelnaga, I. Zewail, and M. Shokair, "Design of 10 × 10 massive MIMO array in a sub-6 GHz smartphone for 5G applications," *Progress in Electromagnetics Research B*, vol. 91, pp. 97-114, 2021.

[2] I. Al-Mejibli and S. Al-Majeed, "Challenges of using MIMO channel technology in 5G wireless communication systems," *IEEE Majan International Conference (MIC)*, pp. 1-5, 2018.

[3] L. Zhang, Q. Feng, and M. K. Khan, "Design of a novel circularly polarized MIMO antenna with enhanced isolation for ultra-wideband communication," *Applied Computational Electromagnetics Society (ACES) Journal*, vol. *37*, pp. 607-618, 2022.

[4] B. Arumita and V. Gupta, "Design and development of low-profile MIMO antenna for 5G new radio smartphone applications," *Wireless Personal Communications,* vol. 111, pp. 1695-1706, 2020.

[5] *5G NR specifications*, document TS 38.101-1 V15.4.0, (3GPP Release 15, 2018).

[6] L. Yixin, Y. Luo, and G. Yang, "Multiband 10-antenna array for sub-6 GHz MIMO applications in 5-G smartphones," *IEEE Access,* vol. 6, pp. 28041-28053, 2018.

[7] L. Kai-Chi, C. Wu, C. Lai, and T. Ma, "Novel dual-band decoupling network for two-element closely spaced array using synthesized microstrip lines," *IEEE Transactions on Antennas and Propagation*, vol. 60, pp. 5118-5128, 2012.

[8] C. Hassan, "Compact high isolation wideband 4G and 5G multi-input multi-output antenna system for handheld and internet of things applications," *International Journal of RF and Microwave Computer-Aided Engineering*, vol. 29, 2019.

[9] K. Saeed, A. Capobianco, A. Najam, I. Shoaib, E. Autizi, and M. Shafique, "Compact ultra-wideband diversity antenna with a floating parasitic digitated decoupling structure," *IET Microwaves, Antennas and Propagation*, vol. 8, pp. 747-753, 2014.

[10] S. Li, S. W. Cheung, and T. I. Yuk, "Compact MIMO antenna for portable UWB applications with band-notched characteristic," *IEEE Transactions on Antennas and Propagation*, vol. 63, pp. 1917-1924, 2015.

[11] D. Helena, M. R. Subasree, S. Susithra, S. S. Keerthika, and B. Manimegalai, "Mutual coupling

reduction in MIMO antenna system using EBG structures," *International Conference on Signal Processing and Communications (SPCOM)*, pp. 1-5, 2012.

[12] B. Anandrao and M. S. Kumbharm, "Wideband circularly polarized conformal strip fed three-layer hemispherical dielectric resonator antenna with parasitic patch," *Microwave and Optical Technology Letters*, vol. 56, pp. 72-77, 2014.

[13] Y. Chenyin, S. Yang, Y. Chen, W. Wang, L. Zhang, B. Li, and L. Wang, "A super-wideband and high isolation MIMO antenna system using a windmill-shaped decoupling structure," *IEEE Access*, vol. 8, pp. 115767-115777, 2020.

[14] I. Tariqul and M. Alam, "Compact EBG structure for alleviating mutual coupling between patch antenna array elements," *Progress in Electromagnetics Research*, vol. 137, pp. 425-438, 2013.

[15] K. Vasu and B. Anuradha, "Design of UWB MIMO antenna to reduce the mutual coupling using defected ground structure," *Wireless Personal Communications*, vol. 118, pp. 3469-3484, 2021.

[16] L. Yingsong, W. Li, C. Liu, and T. Jiang, "Two UWB-MIMO antennas with high isolation using sleeve coupled stepped impedance resonators," *IEEE Asia-Pacific Conference on Antennas and Propagation*, pp. 21-22, 2012.

[17] W. Yan and Z. Du, "A wideband printed dual-antenna system with a novel neutralization line for mobile terminals," *IEEE Antennas and Wireless Propagation Letters*, vol. 12, pp. 1428-1431, 2013.

[18] H. Jian-Rong and J. Li, "Compact microstrip antennas using CSRR structure ground plane," *Microwave and Optical Technology Letters*, vol. 56, no. 1, pp. 117-120, 2014.

[19] D. Chandu, S. Karthikeyan, and K. Kumar, "Reduction of mutual coupling in a two-element patch antenna array using sub-wavelength resonators," *Twenty-First National Conference on Communications (NCC)*, pp. 1-5, 2015.

[20] Y. Hui, J. Ding, C. Guo, Y. Qu, and Y. Song, "A wideband dual-polarized printed antenna based on complementary split-ring resonators," *IEEE Antennas and Wireless Propagation Letters*, vol. 14, pp. 410-413, 2014.

[21] Z. Anping and Z. Ren, "Multiple-input and multiple-output antenna system with self-isolated antenna element for fifth-generation mobile terminals," *Microwave and Optical Technology Letters*, vol. 61, pp. 20-27, 2019.

[22] S. Libin, H. Feng, Y. Li, and Z. Zhang, "Tightly arranged orthogonal mode antenna for 5G MIMO mobile terminal," *Microwave and Optical Technology Letters*, vol. 60, pp. 1751-1756, 2018.

[23] T. G. Abo-Elnaga, D. A. Salem, E. A. F. Abdallah, and H. El-Hennawy, "Wideband rectangular dielectric resonator antenna for S-band applications," *International Symposium on Antennas and Propagation*, pp. 1-6, 2006.

[24] E. Abdallah, T. G. Abo-Elnaga, and H. El-Hennawy, "Ground slotted phi shape UWB stacked circular polarized antenna for 5.8 GHz RFID reader," *Progress in Electromagnetics Research*, vol. 231, 2010.

[25] E. Abdallah, T. G. Abo-Elnaga, and H. El-Hennawy, "Ground slotted landa shape single feed UWB circular polarized antenna for 2.4 GHz RFID reader," *Progress in Electromagnetics Research*, vol. 225, 2010.

[26] S. Mohammad, "Printed multi-band MIMO antenna systems and their performance metrics," *IEEE Antennas and Propagation Magazine*, vol. 55, pp. 218-232, 2013.

[27] N. Jamal, M. Jamaluddin, M. Khalily, M. Kamarudin, I. Ullah, and R. Selvaraju, "A reduced size dual port MIMO DRA with high isolation for 4G applications," *International Journal of RF and Microwave Computer-Aided Engineering*, vol. 25, pp. 495-501, 2015.

Tamer Gaber Abouelnaga was born in Nov. 1976. He received his B.Sc. degree (1994-1999, honors degree) in electronics engineering from Menofiya University, Egypt, M.Sc. degree (2002-2007), and Ph.D. degree (2007-2012) in electronics and communications from Ain Shams University. He works as a researcher (2012-2017) and an associate professor (2018-now) in Microstrip Circuits Department, Electronics Research Institute, Egypt. He works as students affairs vice dean (2018-2019) and community service and environmental development vice dean (2019 till now) at the Higher Institute of Engineering and Technology, Kafr Elsheikh City. He has published 29 papers in peer-refereed journals, and 13 papers in international conferences regarding antennas, couplers, filters, and dividers for different microwave applications.

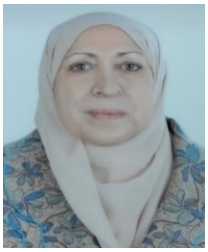

Esmat A. Abdallah (Senior Member, IEEE) graduated from the Faculty of Engineering, Cairo University, Giza, Egypt in 1968. She received her M.Sc. and Ph.D. degrees from Cairo University in 1972, and 1975, respectively. She was nominated as assistant professor, associate professor, and professor in 1975, 1980, and 1985, respectively. In 1989, she was appointed president of the Electronics Research Institute ERI, Cairo, Egypt, a position she held for about ten years. She became the Head of the Microstrip Department, ERI, from 1999 to 2006. Currently, she is at the Microstrip Department, Electronics Research Institute, Cairo, Egypt. She has focused her research on microwave circuit designs, planar antenna systems, and nonreciprocal ferrite devices, and recently on EBG structures, UWB components, and antenna and RFID systems. She acts as a single author and as a coauthor on more than 285 research papers in highly cited international journals and proceedings of international conferences. She has six books and seven patents. She supervised more than 85 Ph.D. and M.Sc. theses. She is a member of the National Council of Communication and Information Technology.